ACS APPLIED MATERIALS & INTERFACES

Research Article

www.acsami.org

Direct Observation and Mechanism for Enhanced Electron Emission in Hydrogen Plasma-Treated Diamond Nanowire Films

Kalpataru Panda,[‡] Kamatchi Jothiramalingam Sankaran,[†] Binaya Kumar Panigrahi,[§] Nyan-Hwa Tai,[†] and I-Nan Lin*[,⊥]

[‡]Graduate School of Engineering, Osaka University, 2-1 Yamada-Oka, 565-0871 Suita, Osaka, Japan

[†]Department of Materials Science and Engineering, National Tsing Hua University, Hsinchu 30013, Taiwan, ROC

[§]Materials Science Group, Indira Gandhi Centre for Atomic Research, Kalpakkam 603 102, India

[⊥]Department of Physics, Tamkang University, Tamsui 251, Taiwan, ROC

ABSTRACT: The effect of hydrogen plasma treatment on the electrical conductivity and electron field emission (EFE) properties for diamond nanowire (DNW) films were systematically investigated. The DNW films were deposited on silicon substrate by N_2-based microwave plasma-enhanced chemical vapor deposition process. Transmission electron microscopy depicted that DNW films mainly consist of wirelike diamond nanocrystals encased in a nanographitic sheath, which formed conduction channels for efficient electron transport and hence lead to excellent electrical conductivity and EFE properties for these films. Hydrogen plasma treatment initially enhanced the electrical conductivity and EFE properties of DNW films and then degraded with an increase in treatment time. Scanning tunneling spectroscopy in current imaging tunneling spectroscopy mode clearly shows significant increase in local emission sites in 10 min hydrogen plasma treated diamond nanowire (DNW10) films as compared to the pristine films that is ascribed to the formation of graphitic phase around the DNWs due to the hydrogen plasma treatment process. The degradation in EFE properties of extended (15 min) hydrogen plasma-treated DNW films was explained by the removal of nanographitic phase surrounding the DNWs. The EFE process of DNW10 films can be turned on at a low field of 4.2 V/μm and achieved a high EFE current density of 5.1 mA/cm^2 at an applied field of 8.5 V/μm. Moreover, DNW10 films with high electrical conductivity of 216 $(\Omega\ \mathrm{cm})^{-1}$ overwhelm that of other kinds of UNCD films and will create a remarkable impact to diamond-based electronics.

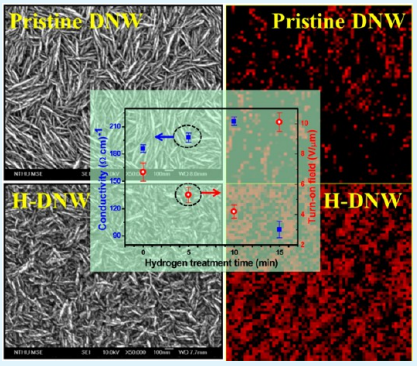

KEYWORDS: *diamond nanowire films, hydrogen plasma treatment, nanographite, electron field emission, scanning tunneling spectroscopy, high resolution transmission electron microscopy,*

1. INTRODUCTION

Field-emission displays (FEDs) are considered to substitute the presently dominant liquid crystals because of their low cost and high performances. However, improvement in consistent and efficient cold cathode materials for electron field emitters is one of the major concerns in FED technology.[1−4] Different nanostructured materials such as semiconducting nanowires or nanotubes, carbon nanotubes (CNTs), diamond films have been demonstrated to show low turn-on voltages and high current density values, making them suitable for cold cathode emitter applications. Among the nanostructured materials, diamond films have attracted considerable interest due to their negative electron affinity (NEA) properties, which make them a suitable promising material for application in FED technologies.[5−9]

It is well recognized that surfaces of diamond films play an important role in the emission characteristics.[10−12] When the surface of diamond films is bonded with different atoms, the resulting band structure below the surface is altered and changes the emission properties. Various surface treatments have been conducted to enhance the field-emission properties of diamond films. Fe-coating and subsequent post-annealing is seen to enhance the EFE properties of diamond films.[13,14] Other studies show monolayer coatings of metals such as Co, Ni, Cu, Zr improved the emission properties of diamond films by shifting the position of the vacuum level.[15,16] It has been also reported that hydrogen treatment of diamond surfaces results in enhanced EFE properties.[17] In the last few year,s the study of hydrogenated diamond surfaces has been a topic of great interest. This is motivated by the fact that when hydrogen is chemisorbed on the diamond surface, its surface electronic structure is modified significantly. Hydrogen plasma treatment not only etches the nondiamond carbon contents, but also gives a NEA surface with better conductivity and emission properties.

On the other hand, varieties of one-dimensional (1D) materials have been successfully synthesized[18,19] since the discovery of CNTs in 1991.[20] Among those 1D materials, diamond nanowires (DNWs) are of great interest because

Received: March 8, 2014
Accepted: May 13, 2014
Published: May 13, 2014

   dx.doi.org/10.1021/am501398s | ACS Appl. Mater. Interfaces 2014, 6, 8531−8541

theoretical studies and simulations explained their structural stabilities and inspire several potential applications.[21−23] They are intrinsically dependent on the size and crystallographic directions and found to be energetically favored and structurally stable at diameters ranging from 2.7 to 9.0 nm.[21,22] The DNW precursor from porous diamond films was successfully fabricated by reactive ion etching in O_2 and CF_4 plasma.[24] Recently, DNWs of 80−100 nm in length were synthesized in ultrananocrystalline diamond (UNCD) films by microwave plasma-enhanced chemical-vapor deposition (MPECVD) process.[25,26]

Until now, the investigation of hydrogen plasma treatment on the emission properties of these new carbon materials, DNW films, has not been studied. In addition, an examination of hydrogen plasma treatment for DNW films is not only expected to give an improvement in emission properties but also to understand the electrical conductivity and emission mechanism. Moreover, better electrical conductivity has been observed for UNCD films when they are prepared in a N_2 rich plasma medium.[25,26] Additionally, the incorporation of N_2 transformed the randomly oriented 3−5 nm diamond crystallites of UNCD to diamond nanowires surrounded by a largely sp^2-bonded carbon sheath that favors the electron transport in pristine DNW films. However, the electrical conductivity and EFE properties for these materials are still not satisfactory implying the fact that most of the DNW surfaces do not have the sp^2-like carbon sheath. An attempt has been made to further improve and understand the mechanism for enhanced electrical conductivity and electron emission characteristics by simple hydrogen plasma treatment.

In the present work, we report a systematic study on the electron field emission and conductivity properties of hydrogen plasma treated DNW films. Structural properties, surface morphology, and field emission properties, along with possible field emission mechanisms for these films have been investigated in detail. The field emission behavior is explained in terms of microstructure and nanocrystalline graphite content of these films. Moreover, scanning tunneling microscopy (STM) is used to detect the emission sites and the mechanism for enhanced EFE properties from a microscopic viewpoint. The conducting regimes at both on the DNW and DNW grain boundaries were examined by scanning tunneling spectroscopy (STS) in more detail.

2. EXPERIMENTAL SECTION

DNW films with a thickness of 700 nm were deposited on mirror polished N-type silicon (100) substrates in N_2 (94%)/CH_4 (6%) plasma by MPECVD (IPLAS-CYRANNUS) system, with a microwave power and frequency of 1200 W and 2.45 GHz, respectively. During the deposition, the chamber pressure was maintained at 70 mbar and total flow rate of gases was 100 sccm. To create nucleation sites prior to the deposition of DNW films, the silicon substrates were ultrasonicated in a methanol solution containing nanodiamond powders (30 nm) and titanium powders (325 mesh) for 45 min. During the DNW growth, the Si substrate was heated using an external heater to a temperature of 700 °C, which was monitored by a thermocouple (*K*-type) embedded in the stainless steel substrate holder. After the deposition of the DNW films, they were post-treated by hydrogen plasma of 100 sccm for 5, 10, and 15 min at a pressure of 7 mbar with a microwave power of 600 W. During hydrogen plasma processing, the plasma temperature was kept at 600 °C for all DNW films. Thus, obtained films were designated as "DNW5", "DNW10", and "DNW15," respectively, whereas the pristine DNW films were designated as "DNW0".

Morphological and microstructural characterizations of the films were examined using field emission scanning electron microscopy (FESEM; JEOL 6500) and transmission electron microscopy (TEM; JEOL 2100, 200 eV), respectively. The plane-view TEM samples were prepared by mechanical grinding, followed by dimpling and Ar-ion milling. The preparation for cross-sectional TEM specimens is usually carried out by fabricating a sandwich structure and subsequently thinning until it becomes transparent for electron. The bonding structure of these films were characterized at room temperature using Raman spectroscopy (Lab Raman HR800, Jobin Yvon), with a wavelength of 632.8 nm and X-ray photoelectron spectroscopy (XPS). XPS with an energy resolution of 0.5 eV, has a SPECS make photoelectron spectrometer, which uses monochromatic Al Kα radiation at 1486.74 eV as the probe. The "phoibos 150″ 9-channel detector from SPECS has been used as an analyzer. Hall measurements (ECOPIA HMS-3000) were carried out in the van der Pauw configuration to measure the conductivities of pristine and hydrogen plasma-treated DNW films. Field emission measurements were carried out in a tunable parallel plate setup, in which the cathode (DNW films) to anode (tip, a Molybdenum rod with a diameter of 2 mm) distance is controlled by a micrometer and an optical microscope. The DNW films that act as a cathode mounted on copper plate sits on the platform of the emission unit. This whole unit is placed in vacuum. The negative terminal of the high voltage source (1KV) is connected to the DNW films where voltage is supplied for electron emission measurements. The EFE properties were analyzed by the Fowler−Nordheim (F−N) model.[27]

$$J = AE^2 \exp\left[\frac{-B\varphi^{3/2}}{E}\right]$$

$$\text{where } A = e^3/16\pi^2 h\varphi t^2(y_0) \text{ and } B = \frac{4}{3e}\left(\frac{2m}{h^2}\right)^{1/2} \nu(y_0)$$

where φ is the work function of the emitting materials. J and E are EFE current density and applied field, respectively. The turn-on field (E_0) was designated as the interception of the lines extrapolated from the high-field and low-field segments of the F−N plot. The local EFE behavior was investigated elaborately by scanning tunneling microscopy (STM; 150 Aarhus, SPECS GmbH) in ultrahigh vacuum (1×10^{-10} mbar) at room temperature. STM tips were prepared by electrochemical etching of tungsten wires of diameter 0.3 mm. STM images were taken in a constant current mode with a set current of 0.58 nA and a bias voltage of −3 V. Current image tunneling spectra (CITS) with voltages ramping from −5 to 5 V were measured simultaneously during the STM image scanning.

3. RESULTS

3.1. Materials Characterization. Figure 1a shows the J versus E characteristics of pristine and hydrogen treated DNW films, whereas the inset of the figure is the F−N plots of the corresponding J−E curves. For the DNW0 films (curve I, Figure 1a), E_0 shows a higher value of 6.8 V/μm with a lower J value of 0.4 mA/cm^2 at an electric field of 8.5 V/μm. The E_0 value decreases consistently with the hydrogen plasma treatment time. The best EFE properties are observed for DNW10 films with a lower E_0 value of 4.2 V/μm and a higher J value of 5.1 mA/cm^2 at an electric field of 8.5 V/μm. These EFE parameters, including E_0 and J values with the percentage of error in measurements are listed in Table 1a. However, increasing the hydrogen treatment time further to 15 min surprisingly degrades the EFE properties, i.e., E_0 value increased to 10.1 V/μm with a sudden decrease in J value to 0.01 mA/cm^2 at an applied field of 8.5 V/μm. Moreover, the DNW10 films exhibit far better EFE properties of lower E_0 and higher J values than that of other diamond related materials reported recently[28−34] and comparable to the carbon-based

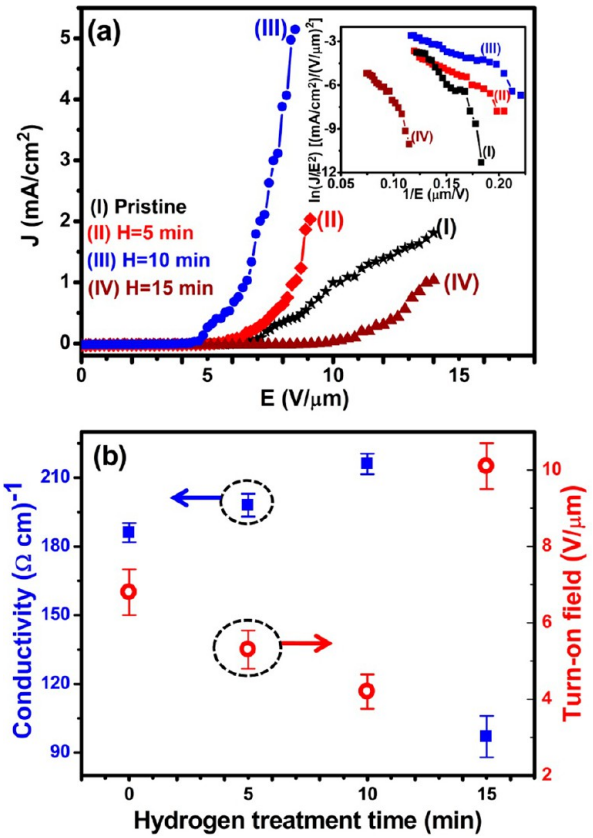

Figure 1. (a) Electric field emission current density (J) as a function of applied electric field (E) for (I) pristine, (II) 5 min, (III) 10 min, and (IV) 15 min hydrogen plasma-treated DNW films. The F–N plot $\ln(J/E^2) - 1/E$ are presented in the inset. (b) Variation in the electrical conductivity (solid squares) and turn-on field (open circles) with hydrogen treatment time.

materials.[35−39] Hall measurements in van der Pauw configuration were taken on pristine and hydrogen treated DNWs films at room temperature. Figure 1b shows the electrical conductivity values of these films as a function of hydrogen treatment time along with the corresponding E_0 values for each sample. The error in measurement of electrical conductivity and E_0 values of pristine and hydrogen plasma treated DNW films is shown in this figure. Interestingly, the conductivity for DNW films increases monotonously upon hydrogen plasma treatment time up to 10 min and suddenly dropped upon longer hydrogen plasma treatment for DNW15 films. Superior EFE properties (i.e., lower E_0 and higher J) observed in DNW10 films are closely related to the better electrical conductivity of these films.

The plane-view FESEM micrographs of pristine and hydrogen plasma treated DNW films are shown in Figure 2. It can be observed that DNW0 films (Figure 2a) possess wirelike granular structure that was dense and uniformly distributed. Further, the wirelike morphology starts to break into finer grains after hydrogen plasma treatment for 5 and 10 min as noticed in images b and c in Figure 2 for DNW5 and DNW10, respectively. The grains of DNW15 film become random/spherical shape due to 15 min hydrogen plasma treatment (Figure 2d). Raman spectroscopy was used to examine the structural changes in the DNW films treated in hydrogen atmosphere and the spectra are shown in Figure 3. Curve I of Figure 3a shows the spectrum of DNW0 films with a

Table 1. Electrical Conductivity and EFE Properties for (a) Pristine and Hydrogen Plasma-Treated DNW Films and (b) EFE Properties of Other Carbon Materials for Comparison

samples	electrical conductivity $(\Omega\ cm)^{-1}$ (% error)	turn-on field E_0 (V/μm) (% error)	current density J (mA/cm²) (% error)
	(a) present study		
DNW0	186 (7.5)	6.8 (7.8)	0.4 (8) @ 8.5 V/μm
DNW5	198 (8.9)	5.3 (8)	1 (9.2) @ 8.5 V/μm
DNW10	216 (9.1)	4.2 (4.9)	5.1 (7.5) @ 8.5 V/μm
DNW15	97 (8.9)	10.1 (5.7)	0.01 (5.6) @ 8.5 V/μm
	(b) reported results		
H-treated diamond film[28]		1.5	1 μA/cm² @ 1.5 V/μm
Au-UNCD[29]	186	4.5	6.70 @ 7.8 V/μm
UNCD film[30]		8.69	0.35 @ 50 V/μm
Li-doped UNCD[31]	7.4×10^{-3}	12	0.20 @ 20.0 V/μm
c-diamond and n-diamond grains on Si nanoneedles[32]		2.2	2.2 mA/cm² @ 14 V/μm
N-implanted UNCD[33]		13	6.4 mA/cm² @ 50 V/μm
Cu ion implanted UNCD/annealing[34]	95	4.8	3.6 mA/cm² @ 8 V/μm
CNT–graphene hybrid material[35]		2.9	1.2 mA/cm² @ 4 V/μm
open-ended tubular graphite cones[36]		1.8	0.65 mA/cm²
coral-like CNTs[37]		4.0	
CNT/TEOS[38]		1.76	0.5 mA/cm² @ 2.7 V/μm
metallic nanowire/graphene hybrid nanostructures[39]		7	300 μA/cm² @ 2.5 V/μm

broad peak at approximately 1120 cm^{-1} corresponding to the trans-polyacetylene (TPA) phase and marks an alternate chain of sp^2 bonded carbon atoms with single hydrogen bonding to each carbon atom.[40−42] The disordered carbon (D* band) is at approximately 1334 cm^{-1}, and the graphite (G peak) at approximately 1594 cm^{-1}. From Figure 3, it is observed that the D* and G peaks of hydrogen plasma-treated DNW films show some red-shifting with respect to that of DNW0 films. The red-shifting of these peaks are considerable in DNW15 films, i.e., D* peak from 1334 to 1322 cm^{-1} and G peak from 1594 to 1562 cm^{-1}, respectively. It is speculated that the red-shifting of D* and G peaks in DNW15 films is due to etching of the sp^2-bonded carbon atom on the DNW surface by atomic hydrogen[43,44] that will be further discussed shortly.

To understand how hydrogen plasma treatment attributes to the chemical bonding state of DNW films more precisely, we have carried out XPS measurements. The C 1s photoemission spectrum of the pristine and the hydrogen plasma-treated DNW films are shown in Figure 4. The C 1s peak position in diamond is 285.5 eV that is about 1.35 eV higher than that in graphite (284.15 eV).[45−47] If the C 1s core-level binding energies of sp^3 and sp^2 hybrids in pristine and hydrogen-treated DNW films are different, the C 1s peak position will vary. Interestingly, the shift of the C 1s peak position towards lower binding energy side (graphitic phase) is obvious in DNW10

dx.doi.org/10.1021/am501398s | ACS Appl. Mater. Interfaces 2014, 6, 8531−8541

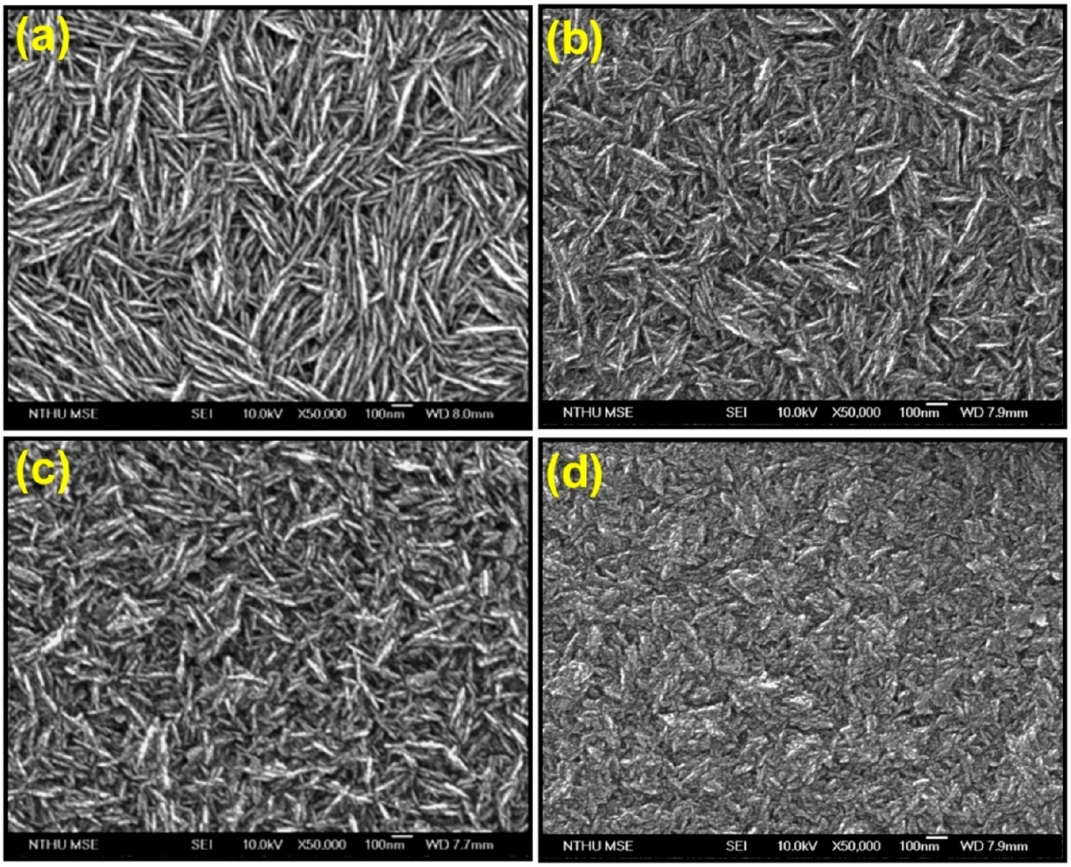

Figure 2. FESEM images of (a) pristine and (b–d) hydrogen plasma-treated DNW films for (b) 5, (c) 10, and (d) 15 min. Significant changes in the surface morphologies are observed after the hydrogen plasma treatment of DNW films.

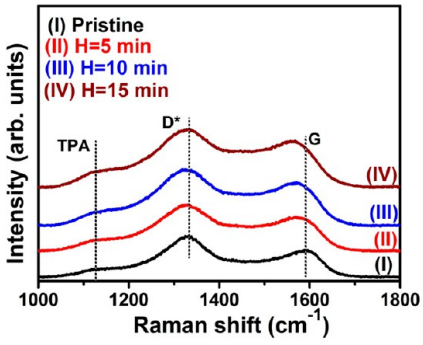

Figure 3. Raman spectra of (I) pristine and (II, III, IV) hydrogen plasma-treated DNW films for (II) 5, (III) 10, and (IV) 15 min.

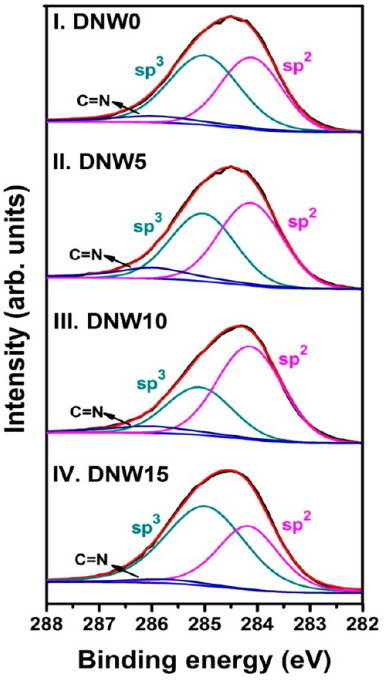

Figure 4. XPS spectra of (I) pristine and (II, III, IV) hydrogen plasma-treated DNW films for (II) 5, (III) 10, and (IV) 15 min.

films indicating more sp^2 graphitic phase content in these films. However, extended hydrogen plasma treatment removes the graphitic content from the DNW15 film surface and C 1s spectra shift towards the diamond side as seen in Figure 4. Diaz et al.[48,49] also proposed a sp^3 and sp^2 identification method by assuming a higher binding energy due to sp^3 hybrids. Therefore, the data were fitted with Lorentzian peaks with binding energies at 284.1, 285.1, and 286.0 eV corresponding to sp^2 C═C, sp^3 C−C, and C═N bonding and their relative intensities are tabulated in Table 2. In DNW0 film, sp^3 C−C bonding is predominant with a peak intensity of 49.5%, while sp^2 C═C peak intensity is 41.4% (curve I, Figure 4). The C═N peak is seen with an intensity of 9.1% at binding energy of 286 eV. Interestingly, a significant increase in sp^2 phase fraction due to hydrogen plasma treatment is observed, i.e., the sp^2 C═C peak intensity increases to 49.2% for DNW5 films (curve II, Figure 4) and 62.2% is observed for DNW10 films (curve III,

dx.doi.org/10.1021/am501398s | ACS Appl. Mater. Interfaces 2014, 6, 8531−8541

Table 2. Relative Intensities of Various Components of C 1s XPS Spectra from Pristine and Hydrogen Plasma Treated DNW Films

peak position (eV)	chemical bonding	peak intensity (%)			
		DNW0	DNW5	DNW10	DNW15
284.2	sp^2 C═C	41.4	49.2	64.2	36.2
285.1	sp^3 C−C	49.5	39.0	28.3	59.5
286.0	C═N	9.1	11.8	7.5	4.3

Figure 4). However, extended hydrogen plasma treatment (> 15 min) degrades the graphitic phase content from the DNW surface (curve IV, Figure 4) with sp^2 C═C peak intensity decreased to 36.2%.

3.2. Scanning Tunneling Microscopy. For the purpose of understanding how hydrogen plasma treatment affects the EFE properties for DNW films, the local electrical properties of DNW0 and DNW10 films were investigated by STM. Figure 5a shows the STM image of DNW0 film with its corresponding CITS image in Figure 5b. The wirelike diamond grains (cf. Figure 2a) were observed to consist of aligned small spherical clusters about 50 nm in size. The spherical clusters are presumably sp^2-bonded carbons encasing the wire-like diamond core, forming sp^2-bonded shell, which will be more clearly illustrated in TEM micrograph shortly. Typical DNW grains are marked as "1", "3", and "5" with the corresponding adjacent grain boundaries as "2", "4", and "6" in Figure 5a. The CITS image was taken at a negative bias of 3 V to the sample, showing bright and dark contrast. Bright contrast in the CITS image shows better electron emission sites.[14,33] The dark contrast corresponds to the diamond grains (points "1", "3", and "5") and the bright contrast corresponds to grain boundaries (points "2", "4", and "6"). Thus, in DNW0 films, few emission sites mostly from the DNW grain boundaries are seen. The STM image of DNW10 film is shown in Figure 6a with the corresponding CITS mapping shown in Figure 6b, which was taken at the same negative sample bias of 3 V. The nanosized sp^2-bonded clusters were observed to fuse together that is presumed to be the graphitization of amorphous carbon (*a*-C) phase located in between graphite clusters, which will be further demonstrated in a TEM micrograph shortly. The surface roughness of DNW10 films is observed to be higher than that of DNW0 films. The increase in width of the DNW seen in Figure 6a that is in accord with the FESEM observation (cf. Figure 2c). Again, typical DNW grains are marked as "1", "3", and "5" with the corresponding adjacent grain boundaries as "2", "4", and "6" in Figure 6a and the high emission sites are mostly from the DNW grain boundaries. It is evident that the number densities of high emission sites are significantly enhanced in DNW10 films (by comparing Figure 6b with Figure 5b). Here it is to be noted that the density of conductivity sites in DNW10 films are even better than that of the DNW5 and DNW15 films (data not shown here). These observations are in accord with the superior EFE properties of DNW10 films (Figure 1) than other DNW films. The high-resolution STM (HRSTM) image of DNW10 films with the corresponding CITS mapping, taken at the same negative bias of 3 V to the sample are shown in panels c and d in Figure 6, respectively. The CITS mapping illustrates more clearly that high emission sites are mostly seen from the boundaries of the DNWs, as seen in Figure 6d.

Local *I*−*V* spectra are taken separately on the top of a DNW and on the boundary adjacent to the DNW as shown in Figure 6e. Interestingly, the tunneling current at the grain boundary position (curve i) is much larger than that of the diamond grain position (curve ii). The tunneling current at the DNW grain boundaries demonstrates a tunneling current higher than 52 nA at −1 V comparing to that of the DNW grains (0.28 nA at −1 V). These observations illustrate again the high conductive sites of DNW grain boundaries than that on the DNW grains in a microscopic scale.

3.3. Transmission Electron Microscopy. TEM measurements of DNW0, DNW10, and DNW15 films have been carried out in more detailed to unravel how the structure of DNW films was altered after the hydrogen plasma treatment that greatly affects the electrical conductivity and the EFE properties. Figure 7a shows a typical bright-field (BF) TEM micrograph of DNW0 films, revealing uniformly distributed wirelike morphology. These randomly oriented DNWs have lengths of around 50−200 nm with a few nanometers in diameter. The selected area electron diffraction (SAED) pattern corresponding to DNW0 film is shown in inset of Figure 7a, which exhibits ring-shaped patterns, implying again random orientation of DNWs. The lattice plane spacing, calculated from the SAED pattern of (311), (220), and (111) planes are estimated to be 0.11, 0.12, and 0.21 nm, respectively, which are in line with the crystalline diamond structure. On the other

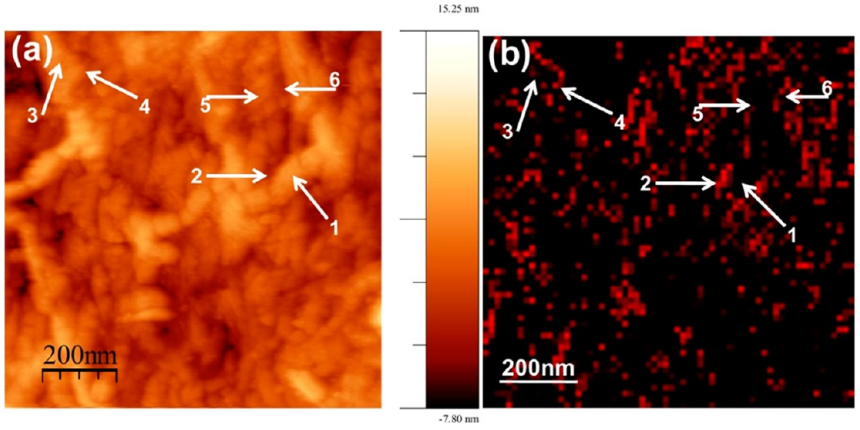

Figure 5. STM micrograph of (a) DNW0 films with (b) the corresponding CITS mapping. Arrow-marked positions "1", "3", "5" and "2", "4", "6"correspond to DNW grains and grain boundaries, respectively, of DNW0 films.

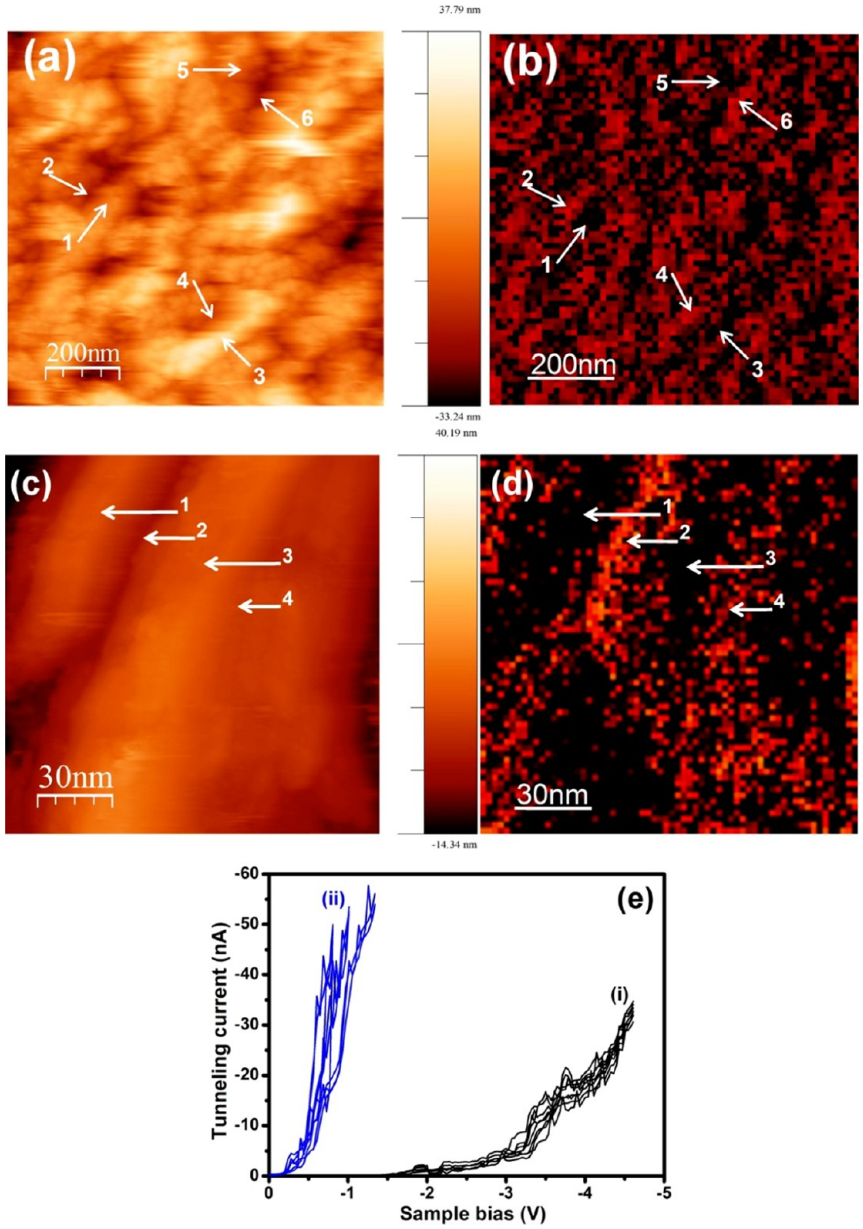

Figure 6. STM micrograph of (a) 10 min hydrogen plasma-treated film with (b) the corresponding CITS mapping. Arrow marked positions "1", "3", "5" and "2", "4", "6"correspond to DNW grains and grain boundaries, respectively, of 10 min hydrogen plasma treated DNWs. HRSTM micrograph of (c) 10 min hydrogen plasma treated DNW with (d) the corresponding CITS mapping. (e) Local $I-V$ characteristic curves at the (i) grain and (ii) grain boundary of DNW10 film clearly showing enhanced conductivity at the DNW grain boundary.

hand, there is a prominent diffused ring in the center of the SAED pattern, signifying the existence of graphitic (or *a*-C) phase in DNW0 film. Similar kind of growth was observed by Arenel et al., in their studies on UNCD films.[25] The TEM structure image of shown in Figure 7b exhibits a clear core–shell microstructure of these DNW films, i.e., DNW is found to be encased by the graphitic phase and the thickness of the graphitic layer is about 4 nm, which contains a few atomic layers with a lattice spacing of 0.34 nm. The core of the DNWs consists of diamond grains with a lattice spacing of 0.21 nm. The diamond and graphitic structures are further analyzed by Fourier transformed (FT) pattern on selective areas. The FT diffractogram (FT_1 image) indicate that the region 1 marked in the HRTEM image (Figure 7b) corresponds to the diamond, while region 2 and 3 corresponds to the graphitic (FT_2 and FT_3 images, Figure 7b) phases. Notably, the crystallinity of nanographitic phase varies markedly along the shell of DNWs. Moreover, there exists large proportion of non-crystalline carbon in the adjacent region. The presence of *a*-C phase coexisting with diamond and graphitic phases away from the DNW are illustrated in region 4 and FT_4 image in Figure 7b.

Marked structural changes have been observed when the DNW0 films are subjected to hydrogen plasma treatment for 10 min. The wirelike granular structure in DNW0 films was transformed to smaller DNW with rodlike geometry, i.e., shorter in length and wider in diameter, as shown in Figure 8a. The appearance of spotty SAED pattern in the inset of Figure 8a indicates better crystalline ordered diamond phase after 10 min hydrogen plasma treatment. HRTEM image of Figure 8b shows that DNWs are broken into smaller DNWs. Besides the better crystallinity for the nanographitic layers encasing the

dx.doi.org/10.1021/am501398s | ACS Appl. Mater. Interfaces 2014, 6, 8531–8541

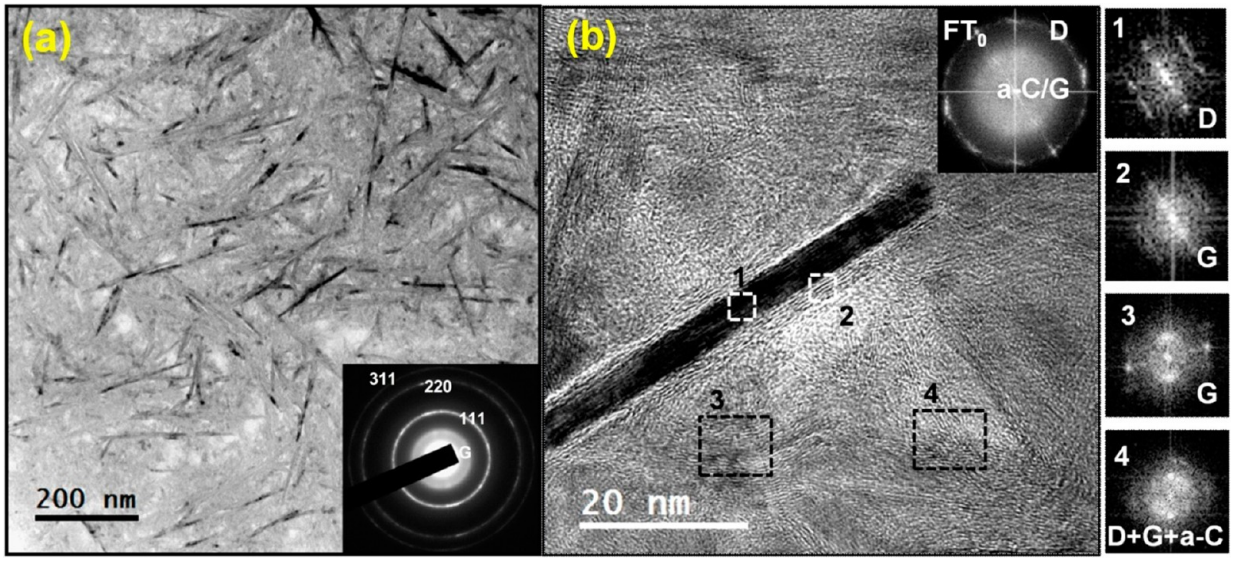

Figure 7. (a) Bright-field TEM image of DNW0 film with inset SAED pattern showing (311), (220), and (111) diffraction rings of diamond and (b) the TEM structure image clearly showing nanowire geometry of diamond phase, encapsulated with graphitic phase. Inset FT images show the phase content at the respective marked area.

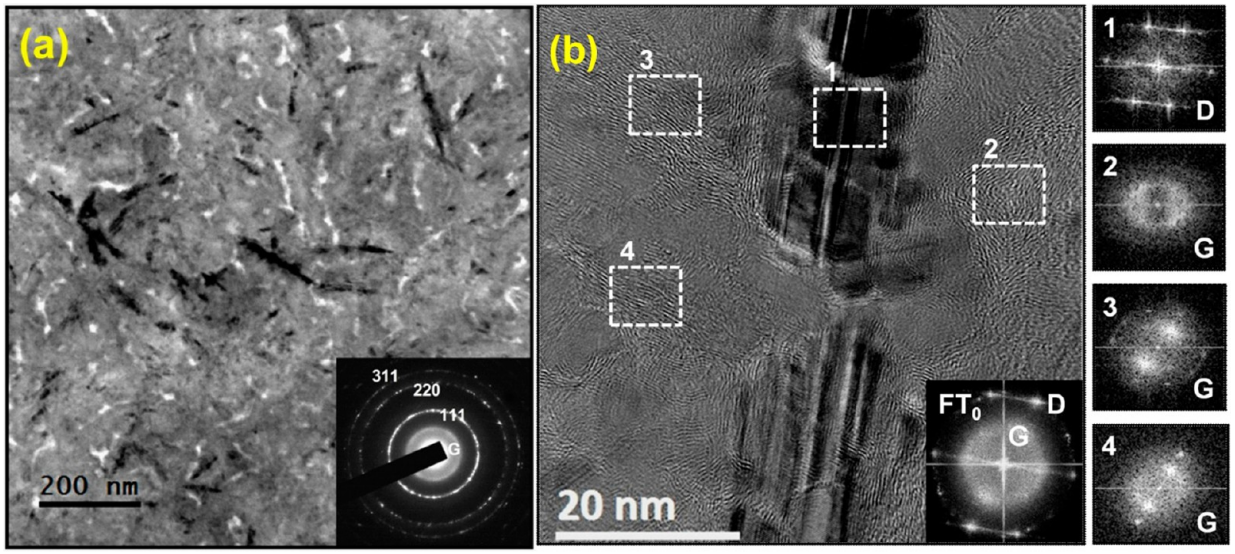

Figure 8. (a) Bright-field TEM image of DNW10 film with inset showing the SAED pattern and (b) the TEM structure image shows nanowire of diamond phase was converted into short rodlike geometry. The inset FT images showing the phase content at the respective marked area.

DNWs, graphitic structure was appeared around most of the DNW domains. FT images (FT_2, FT_3, and FT_4) corresponding to the regions "2", "3", and "4", respectively, in Figure 8b reveals dumbbell-like diffraction spots, indicating clearly that they are graphitic structure. FT_1 image corresponds to the region "1" in Figure 8b exposes the diamond structure of the DNWs. It seems that nanographitic phase was appeared surrounding the DNWs after 10 min hydrogen plasma treatment as seen in Figure 8b.

In contrast, the wirelike granular structure for the diamond grains cannot be observed when the films were subjected to 15 min hydrogen plasma treatment. The low-magnification BF TEM image of DNW15 films (Figure 9a) shows clustered diamond with no wire-like morphology. The inset in Figure 9a shows the corresponding SAED pattern which reveals the diamond structure of these DNW15 grains through the sharp spotted rings (311), (220), and (111) as in DNW0 film (cf. Figure 7a). Moreover, the diffused ring in the center of the SAED pattern is blurred, signifying the appearance of *a*-C phase due to extended hydrogen plasma treatment. The structure image in Figure 9b clearly shows the existence of nanosized diamond grains of about 10−20 nm in size. The core−shell graphite−diamond structure has completely disappeared. The FT images (FT_1−FT_4) shown as the inset of Figure 9b, which correspond to the marked regions of 1−4 in Figure 9b, confirm the presence of *a*-C phases with small proportion of diamond. Therefore, it can be concluded that the graphitic phase around the DNW films has been markedly destroyed after 15 min hydrogen plasma treatment. The TEM examinations of DNW15 films are supportive to the Raman spectroscopy results, which show the red-shift of D* and G peaks as an indication of the formation of *a*-C phase in DNW15 films.

Figure 10 shows the core-loss EELS spectra for DNW0, DNW10, and DNW15 films corresponding to the TEM BF-

dx.doi.org/10.1021/am501398s | ACS Appl. Mater. Interfaces 2014, 6, 8531−8541

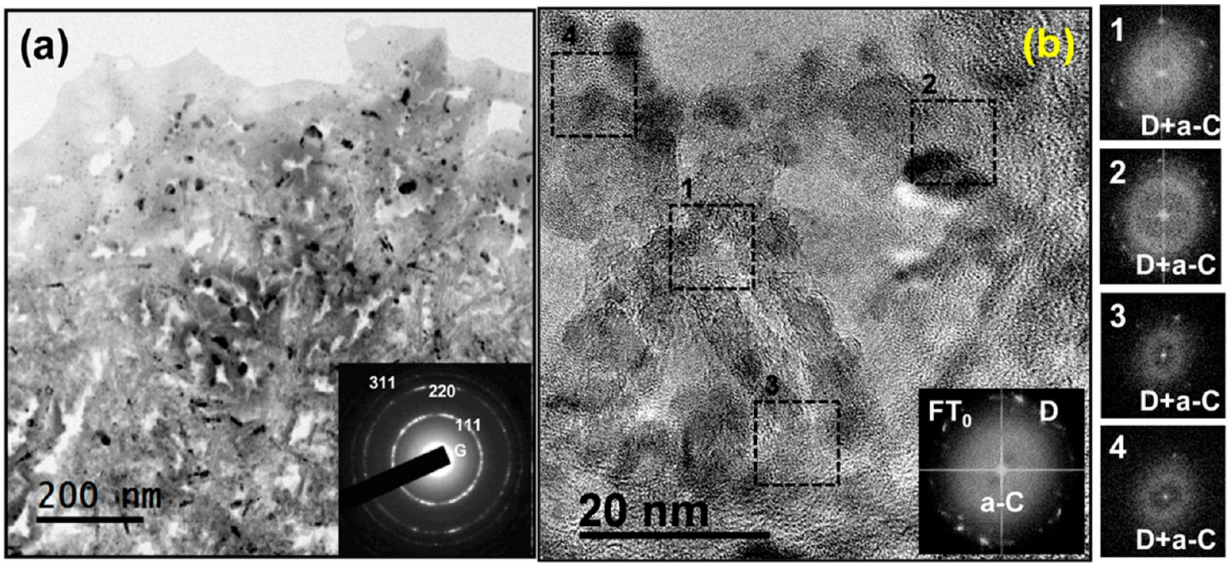

Figure 9. (a) Bright-field TEM image of DNW15 films with inset showing the SAED pattern and (b) the TEM structure image, which shows the disappearance of nanowire morphology. The inset FT images showing the phase content at the respective marked area.

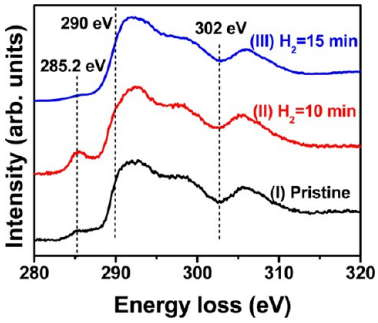

Figure 10. EELS spectra of (I) pristine, and (II, III) hydrogen plasma-treated DNWs for (I) 10 min and (III) 15 min. The appearance of sp^2 graphitic phase at 285.2 eV is clear in DNW10 films.

images in Figures 7a, 8a, and 9a, respectively. All the EELS spectra exhibit a sharp peak around 290.0 eV, corresponding to the transitions from the 1 s to the σ^* energy states (1 s−σ^*), and a dip around 302.0 eV that is a characteristic feature of the crystalline diamond.[50] A week peak at 285.2 eV in curve I for DNW0 films signifies a small fraction of sp^2-bonded phase in DNW0 films (Figure 10). Interestingly, the peak intensity at 285.2 eV significantly increased after 10 min hydrogen plasma treatment (curve II, Figure 10). No signal near 285.2 eV (the π^*-band) was observed in case of DNW15 film (curve III, Figure 10), implying the absence of graphitic sp^2-bonded phase in these films. These observations reveal that, where short time (∼10 min) hydrogen plasma treatment increased markedly the graphitic content of the DNW films, the extended hydrogen plasma treatment time almost destroyed the graphitic content of these films.

4. DISCUSSION

Concerning the origin of the wirelike structure of diamond nanocrystals in DNW0 films, prepared in a N_2-rich plasma condition compared to UNCD films prepared in a Ar-rich plasma, several results are reported.[50−54] It suggests that the changes in the morphology of DNW films prepared in a N_2-rich plasma condition is not the N_2 incorporation in the diamond lattice but nitrogen-related surface processes by the alterations in gas phase chemistry and surface kinetics. The pristine DNW0 film's morphology shown in the TEM micrograph (Figures 7) implies that the nano-diamond grows isotropically in the form of a wire in a N_2/CH_4 plasma. The growth rates along the longitudinal and circumferential directions vary considerably for the films prepared in different substrate temperature (T_S).[55] Moreover, it has been observed that while growing UNCD films in an Ar/CH_4 plasma, which is dominated by C−H and C_2 species,[56] an equiaxed granular structure is obtained, regardless of T_S.[57] Previous studies[53] observe that for sufficiently high T_S (T_S = 700 °C), the granular structure changes from equiaxed for a plasma containing a small proportion of N2 (<5%, with small CN peaks in OES) to an acicular one for a plasma containing a large proportion of N_2 (>10%, with large CN peaks in OES). These observations, in conjunction with the above-described results and XPS measurements (Figure 4) imply strongly that the presence of CN species in the plasma is of critical importance, in addition to a suitable T_S, to form the wirelike DNW structure of UNCD grains. Interestingly, the DNW films have improved EFE properties than the pristine UNCD films. Moreover, hydrogen plasma treatment further enhanced the EFE properties of DNW films. However, up to now, little has been known about the details of the microstructure of the hydrogen plasma-treated diamond films that enhance the conductivity and EFE properties, especially when the diamond grains are of wirelike geometry and encased in graphitic shell. TEM investigations revealed that DNW0 films possess a unique granular structure, viz. with high aspect ratio DNWs as core which was encased in a graphitic shell. The high conductivity graphitic sheath is the prime factor, resulting in high conductivity of the materials that, in turn, leads to outstanding EFE properties for the films. Therefore, the electrical behavior of the graphitic shell is the predominating factor, which resulted in the overall EFE properties of the films. The STS/CITS investigations revealed that the electrons were mainly emitted from the boundaries of DNW. But the DNWs were completely encased by graphitic phase, how can such a phenomenon be happen? The possible explanation on this phenomenon is that on top of DNWs, the graphitic lattice planes are faced on, whereas in the boundaries,

the graphitic lattice planes are edge on, with respect to the applied field. Only the dangling bonds in edge of hexagon graphitic lattices are good conductive sites that result in boundaries of DNWs more emissive than the DNWs themselves.

The other question remaining now is why hydrogen plasma treatment process altered the characteristics of the graphitic sheath of the DNW films and modified their EFE properties? To understand the phenomenon, we depicted the evolution of microstructure of DNW films based on the TEM/EELS observations that is schematically illustrated in Figure 11. In

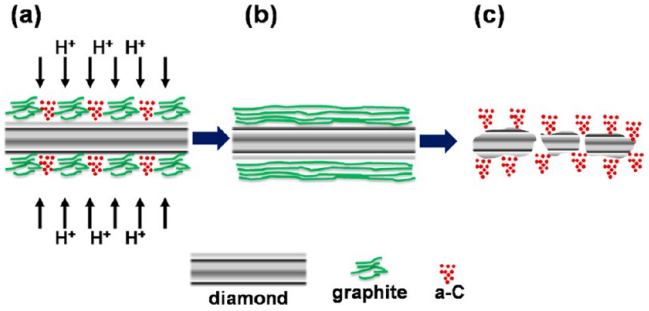

Figure 11. Schematic diagrams showing the effect of hydrogen plasma treatment on modifying the microstructure of DNW films (a) pristine DNWs, (b) 10 min hydrogen plasma treated, and (c) the extended (>15 min) hydrogen plasma-treated DNWs.

the sp^2-bonded phase encasing the wirelike diamond grains for the DNW0 films, there are abundant *a*-C phases, co-existing with the graphitic layers (Figure 11a). When these DNWs were exposed to hydrogen plasma, the hydrogen terminated on the *a*-C phases were abstracted due to the presence of atomic hydrogen in the hydrogen plasma, leaving behind the reactive dangling bond on newly formed carbon, which formed double bonds with the other dangling bond instantaneously, resulting in the formation of graphitic phase as depicted in Figure 11b that enhanced markedly electrical conductivity and EFE behaviors for DNW10 films. The increase in graphitic phase in diamond films after hydrogen beam irradiation is also seen in EELS spectra by Kushita et al.[58] Atomic hydrogen contained in hydrogen plasma is a very aggressive species, which is capable of etching both the sp^2- and sp^3-bonded carbons. Therefore, when the DNWs were kept in hydrogen plasma for longer time, not only did the graphitic phases disappear but also the wirelike diamond started to breakdown into smaller pieces, as depicted in Figure 11c, which accounts for the degradation of both the electrical conductivity and the EFE properties for DNW15 films.

5. CONCLUSIONS

A possible way of fabricating highly field emitting DNW films by simple hydrogen plasma treatment technique is demonstrated. Electrical conductivities and field emission properties are initially enhanced and then degraded with an increase in hydrogen plasma treatment time and the best EFE properties are obtained for 10 min hydrogen plasma treatment. STS in CITS mode clearly shows significant high conductive sites in DNW10 films as compared to DNW0 films. TEM/EELS investigations revealed that the 10 min hydrogen plasma treatment converted the a-*C* phase into nanographitic sp^2 phase. The availability of abundant nanographitic sp^2 phase content around the diamond nanowire in DNW10 films can form interconnected paths throughout the films that facilitated the easy transport of electrons and enhanced the EFE properties. However, extended hydrogen plasma-treated DNW films such as in DNW15 films, resulted in the removal of graphitic phase surrounding the DNWs, which hinders the transportation of electrons and resulted in inferior EFE properties. The highly conducting hydrogen plasma-treated DNW films with enhanced EFE characteristics may open up a pathway for the development of high-definition flat panel displays or plasma devices.

AUTHOR INFORMATION

Corresponding Author

*E-mail: inanlin@mail.tku.edu.tw.

Notes

The authors declare no competing financial interest.

ACKNOWLEDGMENTS

The authors akcowledge the financial support of National Science Council through Projects NSC 99-2119-M-032-003-MY2 and NSC 101-2221-E-007-064-MY3.

REFERENCES

(1) Zhu, W.; Kochanski, G. P.; Jin, S.; Seilbles, L. Defect-enhanced Electron Field Emission from Chemical Vapor Deposited Diamond. *J. Appl. Phys.* **1995**, *78*, 2707−2711.

(2) De Heer, W. A.; Chatelain, A.; Ugarte, D. A Carbon Nanotube Field-emission Electron Source. *Science* **1995**, *270*, 1179−1180.

(3) Amaratunga, G. A. J.; Silva, S. R. P. Nitrogen Containing Hydrogenated Amorphous Carbon for Thin-film Feld Emission Cathodes. *Appl. Phys. Lett.* **1996**, *68*, 2529−2531.

(4) Sun, M.; Gao, Y.; Zhi, C.; Bando, Y.; Golberg, D. Silicon Multi-branch Nanostructures for Decent Feld Emission and Excellent Electrical Transport. *Nanotechnology* **2011**, *22*, 145705−145611.

(5) Yamaguchi, H.; Masuzawa, T.; Nozue, S.; Kudo, Y.; Saito, I.; Koe, J.; Kudo, M.; Yamada, T.; Takakuwa, Y.; Okano, K. Electron Emission from Conduction Band of Diamond with Negative Electron Affinity. *Phys. Rev. B* **2009**, *80*, 165321−165326.

(6) Geis, M. W.; Efremow, N. N.; Krohn, K. E.; Twichell, J. C.; Lszczarz, T. M.; Kalish, R.; Greer, J. A.; Tabat, M. D. A New Surface Electron-emission Mechanism in Diamond Cathodes. *Nature* **1998**, *393*, 431−435.

(7) Okano, K.; Koizumi, S.; Silva, S. R. P.; Amaratunga, G. A. J. Low Threshold Cold Cathodes Made of Nitrogen Doped Chemical-vapor-deposited Diamond. *Nature* **1996**, *381*, 140−141.

(8) Watanabe, H.; Nebel, C. E.; Shikata, S. Polarization Control of Electron Tunneling into Ferroelectric Surfaces. *Science* **2009**, *324*, 1421−1425.

(9) Himpsel, F. J.; Knapp, J. A.; VanVecten, J. A.; Eastman, D. E. Quantum Photoyield of Diamond(111)−A Stable Negative-affinity Emitter. *Phys. Rev. B* **1979**, *20*, 624−627.

(10) Sankaran, K. J.; Lin, Y. F.; Jian, W. B.; Chen, H.-C.; Panda, K.; Sundaravel, B.; Dong, C.-L.; Tai, N.-H.; Lin, I.-N. Structural and Electrical Properties of Conducting Diamond Nanowires. *ACS Appl. Mater. Interfaces* **2013**, *5*, 1294−1301.

(11) Maier, F.; Riedel, M.; Mantel, B.; Ristein, J.; Ley, L.; et al. A Reply to the Comment by Koslowski, Strohel, and Ziemann. *Phys. Rev. Lett.* **2001**, *87*, 209706.

(12) Koslowski, B.; Strobel, S.; Zeiman, P. Comment on Origin of Surface Conductivity in Diamond. *Phys. Rev. Lett.* **2001**, *87*, 209705.

(13) Panda, K.; Sundaravel, B.; Panigrahi, B.K; Chen, H.-C.; Huang, P.-C.; Shih, W.-C.; Lo, S.-C.; Lin, L. J.; Lee, C.-Y.; Lin, I. N. The Induction of Nanographitic Phase on Fe Coated Diamond Films for the Enhancement in Electron Field Emission Properties. *J. Appl. Phys.* **2013**, *113*, 094305−094314.

(14) Panda, K.; Sundaravel, B.; Panigrahi, B. K.; Huang, P.-C.; Shih, W.-C.; Chen, H. C.; Lin, I.N. Direct Observation and Mechanism of Increased Emission Sites in Fe-coated Microcrystalline Diamond Films. *J. Appl. Phys.* **2012**, *111*, 124309−124318.
(15) Van der Weide, J.; Nemanich, R. J. Influence of Interfacial Hydrogen and Oxygen on the Schottky Barrier Height of Nickel on (111) and (100) Diamond Surfaces. *Phys. Rev. B* **1994**, *48*, 13629−13637.
(16) Baumann, P.K.; Nemanich, R. J. Electron Affinity and Schottky Barrier Height of Metal−diamond (100)„ (111) and (110) Interfaces. *J. Appl. Phys.* **1998**, *83*, 2072−2082.
(17) Cui, J. B.; Stammler, M.; Ristein, J.; Ley, L. Role of Hydrogen on Field Emission from Chemical Vapor Deposited Diamond and Nanocrystalline Diamond Powder. *J. Appl. Phys.* **2000**, *88*, 3667−3673.
(18) Huang, M. H.; Mao, S.; Feick, H.; Yan, H.; Wu, Y.; Kind, H.; Webber, E.; Russo, R.; Yang, Y. Room-Temperature Ultraviolet Nanowire Nanolasers. *Science* **2001**, *292*, 1897−1899.
(19) Ma, D. D. D.; Lee, C. S.; Au, F. C. K.; Tong, S. Y.; Lee, S. T. Small-Diameter Silicon Nanowire Surfaces. *Science* **2003**, *299*, 1874−1877.
(20) Iijima, S. Helical Microtubules of Graphitic Carbon. *Nature* **1998**, *354*, 56−58.
(21) Barnard, A. S.; Russo, S. P.; Snook, I. K. Ab Initio Modeling of Diamond Nanowire Structures. *Nano Lett.* **2003**, *3*, 1323−1328.
(22) Barnard, A. S.; Snook, I. K. Phase Stability of Nanocarbon in One Dimension: Nanotubes versus Diamond Nanowires. *J. Chem. Phys.* **2004**, *120*, 3817−3821.
(23) Wang, C. X.; Yang, G. W. Thermodynamics of Metastable Phase Nucleation at the Nanoscale. *Mater. Sci. Eng., R* **2005**, *49*, 157−202.
(24) Shiomi, H. Reactive Ion Etching of Diamond in O_2 and CF_4 Plasma, and Fabrication of Porous Diamond for Field Emitter Cathodes. *Jpn. J. Appl. Phys.* **1997**, *36*, 7745−7748.
(25) Arenal, R.; Bruno, P.; Miller, D. J.; Bleuel, M.; Lal, J.; Gruen, D. M. Diamond Nanowires and the Insulator-metal Transition in Ultrananocrystalline Diamond Flms. *Phys. Rev. B* **2007**, *75*, 195431−195442.
(26) Arenal, R.; Montagnac, G.; Bruno, P.; Gruen, D. M. Multiwavelength Raman Spectroscopy of Diamond Nanowires Present in N-type Ultrananocrystalline Flms. *Phys. Rev. B* **2007**, *76*, 245316−245322.
(27) Fowler, R. H.; Nordheim, L. Electron Emission in Intense Electric Fields. *Proc. R. Soc. London, Ser. A* **1928**, *119*, 173−181.
(28) Zhu, W.; Kochanski, G. P.; Jin, S. Low-Field Electron Emission from Undoped Nanostructured Diamond. *Science* **1998**, *282*, 1471−1473.
(29) Sankaran, K. J.; Chen, H. C.; Sundaravel, B.; Lee, C. Y.; Tai, N. H.; Lin, I. N. Gold Ion Implantation Induced High Conductivity and Enhanced Electron Field Emission Properties in Ultrananocrystalline Diamond Films. *Appl. Phys. Lett.* **2013**, *102*, 061604−061608.
(30) Pradhan, D.; Lin, I. N. Grain Size Dependent Diamond-nondiamond Composite Films: Characterization and Field-emission Properties. *ACS Appl. Mater. Interfaces* **2009**, *1*, 1444−1450.
(31) Thomas, J. P.; Chen, H. C.; Tai, N. H.; Lin, I. N. Freestanding Ultrananocrystalline Diamond Films with Homojunction Insulating Layer on Conducting Layer and their High Electron Field Emission Properties. *ACS Appl. Mater. Interfaces* **2011**, *3*, 4007−4013.
(32) Thomas, J. P.; Chen, H. C.; Tseng, S. H.; Wu, H. C.; Lee, C. Y.; Cheng, H. F.; Tai, N. H.; Lin, I. N. Preferentially Grown Ultranano C-diamond and N-diamond Grains on Silicon Nanoneedles from Energetic Species with Enhanced Field-emission Properties. *ACS Appl. Mater. Interfaces* **2012**, *4*, 5103−5108.
(33) Panda, K.; Sundaravel, B.; Panigrahi, B. K.; Magudapathy, P.; Krishna, D. N.; Nair, K. G. M.; Chen, H.-C.; Lin, I.-N. Structural and Electronic Properties of Nitrogen ion Implanted Ultra Nanocrystalline Diamond Surfaces. *J. Appl. Phys.* **2011**, *110*, 044304−044313.
(34) Sankaran, K. J.; Panda, K.; Sundaravel, B.; Tai, N. H.; Lin, I.-N. Enhancing Electrical Conductivity and Electron Field Emission Properties of Ultrananocrystalline Diamond Films by Copper Ion Implantation and Annealing. *J. Appl. Phys.* **2014**, *115*, 063701−063708.
(35) Nguyen, D. D.; Tai, N. H.; Chen, S. Y.; Chueh, Y. L. Controlled Growth of Carbon Nanotube−Graphene Hybrid Materials for Fexible and Transparent Conductors and Electron Field Emitters. *Nanoscale* **2012**, *4*, 632−638.
(36) Shang, N. G.; Papakonstantinou, P.; McLaughlin, J.; Chen, W. C.; Chen, L. C.; Chu, M.; Stamboulis, A. Fe Catalytic Growth, Microstructure, and Low-threshold Field Emission Properties of Open Ended Tubular Graphite Cones. *J. Appl. Phys.* **2008**, *103*, 124308−124312.
(37) Shang, N. G.; Li, C. P.; Wong, W. K.; Lee, C. S.; Bello, I.; Lee, S. T. Microstructure and Field Emission Properties of Coral-like Carbon Nanotubes. *Appl. Phys. Lett.* **2002**, *81*, 5024−5026.
(38) Jeong, H. J.; Jeong, H. D.; Kim, H. Y.; Kim, J. S.; Jeong, S. Y.; Han, J. T.; Bang, D. S.; Lee, G. W. All-Carbon Nanotube-Based Flexible Field-Emission Devices: From Cathode to Anode. *Adv. Funct. Mater.* **2011**, *21*, 1526−1532.
(39) Arif, M.; Heo, K.; Lee, B. Y.; Lee, J.; Seo, D. H.; Seo, S.; Jian, J.; Hong, S. Metallic Nanowire−Graphene Hybrid Nanostructures for Highly Flexible Field Emission Devices. *Nanotechnology* **2011**, *22*, 355709−355716.
(40) Ferrari, A. C.; Robertson, J. Origin of the 1150 cm^{-1} Raman Mode in Nanocrystalline Diamond. *Phys. Rev. B* **2001**, *63*, 121405−121409.
(41) Kuzmany, H.; Pfeiffer, R.; Salk, N.; Günther, B. The Mystery of the 1140 cm^{-1} Raman Line in Nanocrystalline Diamond Films. *Carbon* **2004**, *42*, 911−917.
(42) Ferrari, A. C.; Robertson, J. Interpretation of Raman Spectra of Disordered and Amorphous Carbon. *Phys. Rev. B* **2000**, *61*, 14095−14107.
(43) Shim, J.Y.; Chi, E.J.; Baik, H. K.; Lee, S.M. Structural, Optical, and Field Emission Properties of Hydrogenated Amorphous Carbon Films Grown by Helical Resonator Plasma Enhanced Chemical Vapor Deposition. *Jpn. J. Appl. Phys.* **1998**, *37*, 440−444.
(44) Nagai, I.; Ishitani, A.; Yoshikawa, M.; Nagai, N. Preparation of Diamond Like Carbon Films by Electron Cyclotron Resonance Chemical Vapor Deposition. *J. Appl. Phys.* **1990**, *67*, 2890−2893.
(45) Taki, Y.; Takai, O. XPS Structural Characterization of Hydrogenated Amorphous Carbon Thin Films Prepared by Shielded Arc Ion Plating. *Thin Solid Films.* **1998**, *316*, 45−50.
(46) Bŕuhwiler, P.A.; Maxwell, A.J.; Puglia, C.; Nilsson, A.; Andersson, S.; Artensson, N. M. π^* and σ^* Excitons in C 1s Absorption of Graphite. *Phys. Rev. Lett.* **1995**, *74*, 614−617.
(47) Morar, J. F.; Himpsel, F.J.; Hollinger, G. J.; Jordan, L.; Hughes, G.; McFeely, F.R. C 1s Excitation Studies of Diamond (111).I. Surface Core Levels. *Phys. Rev. B* **1986**, *33*, 1340−1345.
(48) Diaz, J.; Paolicelli, G.; Ferrer, S.; Comin, F. Separation of the sp^3 and sp^2 Components in the C 1s Photoemission Spectra of Amorphous Carbon Films. *Phys. Rev. B* **1996**, *54*, 8064−8069.
(49) Diaz, J.; Martin-Gago, J. A.; Ferrer, S.; Comin, F.; Abello, L.; Loucazeau, G. Raman Spectroscopy of Carbon Films Grown by Pulsed Laser Evaporation of Graphite. *Diamond Relat. Mater.* **1992**, *1*, 824−827.
(50) Chu, P. K.; Li, L. Characterization of Amorphous and Nanocrystalline Carbon Films. *Mater. Chem. Phys.* **2006**, *96*, 253−277.
(51) Sobia, A. R.; Yu, G.; Cao, J.; He, S.; Zhou, X. Influence of CH4 on the Morphology of Nanocrystalline Diamond Films Deposited by Ar-rich Microwave Plasma. *J. Appl. Phys.* **2010**, *107*, 114324−114328.
(52) Shang, N.; Papakonstantinou, P.; Wang, P.; Zakharov, A.; Palnitkar, U.; Lin, I.-N.; Chu, M.; Stamboulis, A. Self-Assembled Growth, Microstructure, and Field-Emission High-Performance of Ultrathin Diamond Nanorods. *ACS Nano* **2009**, *3*, 1032−1038.
(53) Vlasov, I. I.; Lebedev, O. I.; Ralchenko, V. G. Hybrid Diamond-Graphite Nanowires Produced by Microwave Plasma Chemical Vapor Deposition. *Adv. Mater.* **2007**, *19*, 4058−4062.
(54) Cao, G. Z.; Schermer, J. J.; van Enckevort, W. J. P.; Elst, W. A. L. M.; Giling, L. J. Growth of {100} Textured Diamond Films by the Addition of Nitrogen. *J. Appl. Phys.* **1996**, *79*, 1357−1364.
(55) Sankaran, K. J.; Kurian, J.; Chen, H. C.; Dong, C. L.; Lee, C. Y.; Tai, N. H.; Lin, I. N. Origin of a Needle-like Granular Structure for

Ultrananocrystalline Diamond Films Grown in a N_2/CH_4 Plasma. *J. Phys. D: Appl. Phys.* **2012**, *45*, 365303−365312.
(56) Wang, C. S.; Chen, H. C.; Cheng, H. F.; Lin, I. N. Origin of Platelike Granular Structure for the Ultrananocrystalline Diamond Films Synthesized in H_2-Containing Ar/CH_4 Plasma. *J. Appl.Phys.* **2010**, *107*, 034304−034311.
(57) Sankaran, K. J.; Chen, H. C.; Lee, C. Y.; Tai, N. H.; Lin, I. N. Fabrication of Free-standing Highly Conducting Ultrananocrystalline Diamond Films with Enhanced Electron Field Emission Properties. *Appl. Phys. Lett.* **2012**, *101*, 241604−241608.
(58) Kushita, K. N.; Hojou, K.; Furuno, S.; Otsu, H. In situ EELS Observation of Diamond During Hydrogen-ion Bombardment. *J. Nucl. Mater.* **1992**, *191−194*, 346−350.